J Nanopart Res (2016) 18:224
DOI 10.1007/s11051-016-3521-z

RESEARCH PAPER

Soy flour-derived carbon dots: facile preparation, fluorescence enhancement, and sensitive Fe^{3+} detection

Liyang Fang · Qian Xu · Xing Zheng · Weina Zhang · Jingtang Zheng · Mingbo Wu · Wenting Wu

Received: 27 December 2015 / Accepted: 15 July 2016 / Published online: 11 August 2016

Abstract Soy flour-derived carbon quantum dots (C-dots) were successfully synthesized via a facile one-step hydrothermal approach. The as-prepared C-dots exhibit an average diameter of 2.5 nm and the crystalline lattices are consistent with graphitic carbons. Meanwhile, they show strong photoluminescence (quantum yield is 7.85 %), good water solubility, and high photostability. Importantly, structural defects of the C-dots were designed to obtain controllable fluorescence, which was achieved by changing the contents of N defects and O defects of C-dots. Our results indicate that N defects can more effectively enhance the fluorescence emission than O defects. As the preparation temperature increases, the N defects are fine-tuned by substituting for partial O defects, reducing nonradiative recombination and enhancing fluorescence intensity, which is further confirmed by surface passivation. Due to its fine photostability, high sensitivity, and good selectivity for Fe^{3+}, the as-prepared C-dots were used as fluorescence probes for detection of ferric ion. The detection limitation comes to 0.021 μM.

Keywords Soy flour-derived C-dots · Preparation · Luminescence properties · Structural defects · Fluorescence enhancement · Fe^{3+} detection

Electronic supplementary material The online version of this article (doi:10.1007/s11051-016-3521-z) contains supplementary material, which is available to authorized users.

L. Fang · Q. Xu · W. Zhang · J. Zheng (✉) · M. Wu (✉) · W. Wu (✉)
State Key Laboratory of Heavy Oil Processing, China University of Petroleum, Qingdao 266580, Shandong, People's Republic of China
e-mail: jtzheng03@163.com

M. Wu
e-mail: wumb@upc.edu.cn

W. Wu
e-mail: wuwt@upc.edu.cn

X. Zheng
Bei Jing Sinen En-Tech Co., Ltd, Beijing 100080, People's Republic of China

Introduction

Carbon quantum dots (C-dots), which are better alternatives to the traditional organic dyes and semiconductor quantum dots, have inspired their applications in bioimaging (Jung et al. 2010), biochemical analysis (Bai et al. 2011), fluorescent sensors (Dong et al. 2012; Lu et al. 2012; Qu et al. 2012; Zhou et al. 2012), and photocatalysis (Cao et al. 2011; Li et al. 2010; Zhuo et al. 2012) because of their less and nontoxicity, excellent biocompatibility, good photostability, cell membrane permeability, and extraordinary optoelectrical properties (Baker and Baker 2010; Fan et al. 2014; Sun et al. 2006; Zhang et al. 2012; Zheng et al. 2009; Zhu et al. 2012b). However these

applications have been impeded by their poor fluorescence emission. To obtain C-dots with tunable strong fluorescence emission, it is significant to truly understand fluorescent emission origins and study how to control the fluorescent emission. Up to now, although many mechanisms for the fluorescent emission of carbon dots, such as quantum effect (Li et al. 2010), exciton complex (Zhou et al. 2007), aromatic structures(Bourlinos et al. 2008), and edge defects (Wang et al. 2010b) have been proposed, there is no any universal interpretation available in the literature. Especially, the view of fluorescent emission from structural defects has been widely accepted. Different structural defects (e.g., C–O, C=O, C–N, and N–H) can introduce different energy levels in C-dots, making C-dots emit light which varies with excitation energy (Li et al. 2014). However, which kind of defect can more effectively enhance the fluorescence emission is still unclear, and further study on adjusting the fluorescent emission of C-dots by the engineering of structural defects has seldom been done. Therefore, it is especially important for more successful applications of C-dots to research the influence factors of the fluorescence enhancement of C-dots and modulate their emission behaviors.

In recent years, great efforts have been made on developing various cheap, easily available, and nontoxic raw natural biomass, such as grass (Liu et al. 2012), Bombyx mori silk (Wu et al. 2013), orange juice (Sahu et al. 2012), and banana juice (De and Karak 2013), as a carbon source for the preparation of C-dots. Soy bean consisting of carbon, oxygen, nitrogen, and other elements are nontoxic, cheap, and easily available and provide both carbon source and nitrogen source. Considering soy flour nitrogen content of about 5.6 %, which is higher than other raw natural materials such as grass, banana juice, milk, and egg, we expect that soy flour-derived C-dots might introduce more nitrogen into the carbon skeleton and thus might have a high fluorescence quantum yield (QY). Consequently, soy flour is an excellent alternative precursor for the synthesis of nitrogen-doped carbon quantum dots.

In this work, soy flour-derived carbon dots were prepared via a facile one-step hydrothermal approach with the assistance of NaOH. The physical and chemical structures and optical properties of the as-prepared C-dots were studied by X-ray powder diffractometer (XRD), transmission electron microscope (TEM), Fourier transform infrared spectrometer (FT-IR), nuclear magnetic resonance (NMR) spectroscopy, Raman spectrometer, X-ray photoelectron spectroscope (XPS), elemental analysis, UV–Vis absorption spectroscope, and fluorescence spectroscope. Fluorescence quantum yield (QY) of the as-prepared C-dots (7.85 %) is much higher than that of the previously reported soy milk-derived C-dots (2.6 %) (Zhu et al. 2012a). The as-prepared C-dots are monodisperse with relatively narrow size distribution from 1.5 to 4 nm and possess highly crystalline nature which is significantly different from certain carbon quantum dots with amorphous or semicrystalline nature (Hu et al. 2014; Sun et al. 2013a; Xu et al. 2015). And they show strong photoluminescence and high photostability. Further, the relationship of fluorescence enhancement of C-dots and their structural defects was deeply studied through changing the contents of N defects and O defects of C-dots. The degree of structural defect change was controlled by varying the synthesis temperature and further modifying the as-prepared C-dots with ethylenediamine. It is proved concretely that N defects, such as C–N defects and N–H defects, are finely tuned by substituting for partial O defects (e.g., C–O, C=O), reducing nonradiative recombination, and enhancing fluorescence intensity. Due to the high sensitivity and satisfying selectivity, the as-synthesized C-dots were successfully used for the selective recognition of Fe^{3+}.

Experimental section

Synthesis of C-dots

Soy flour was purchased from a supermarket and filtered with a sieve to remove large particles. Sodium hydroxide was used without further purification. Deionized water was used for the preparation of all aqueous solutions. Soy flour (5 g) was dispersed into 0.2 M NaOH aqueous solution (60 mL). After ultrasonication, the suspension was transferred into an 80-mL Teflon-lined stainless-steel autoclave and heated at 200 °C for 3 h, then cooled down to room temperature. The reaction products were centrifuged at 10,000 rpm to remove the sediment, and the supernatant aqueous solution of brown C-dots was obtained for further use. The solution was filtered through a 220-nm membrane to dislodge large carbon

residues. Further purification of the C-dots was conducted through a dialysis membrane (molecular weight cut-off: 1000 Da) for 2 days to remove residual NaOH thoroughly. C-dots were then concentrated and dried under vacuum (60 °C). Finally, the C-dots were obtained and recorded as CDs-200. The schematic illustration of the preparation procedure of C-dots by hydrothermal treatment from soy flour is shown in Fig. 1.

Detection of ferric iron test

C-dots solution (0.2 g/L) was prepared with Tris–HCl buffer (20 mM, pH 7.0). Then a different volume of Fe^{3+} aqueous solution (1×10^{-5} M) was added into the C-dots solution to form mixed solution in which Fe^{3+} concentration is 0, 0.5, 1.0, 1.5, 2.0, 2.5, 3.0, 3.5, 4.0, 4.5, and 5.0 μM, respectively. After that, the fluorescence emission spectra of the mixed solution were measured.

Results and discussion

Synthetic strategies

In this work, soy flour-derived carbon dots (CDs-200) were prepared in NaOH aqueous solution. The fluorescent quantum yield of CDs-200 is 7.85 % higher than that of the C-dots obtained in the absence of NaOH (recorded as c-CDs, 3.91 %) (Table S1). In the FT-IR spectra of the samples (Figure S1), the peak at 1532 cm^{-1} can be ascribed to the Amide II band, which CDs-200 have but c-CDs have not. XPS spectra (Figure S2) show that the nitrogen content of CDs-200 is more than that of c-CDs. Therefore, the synthesis of C-dots based on hydrothermal treatment from soy flour under alkaline conditions provides a simple and effective preparation method of nitrogen-doped C-dots.

Meanwhile, a preparation condition of C-dots was optimized under different hydrothermal temperatures from 160 to 240 °C, which were recorded as CDs-160 and CDs-240, respectively. In general, when the temperature is lower than carbonization temperature at which carbon nuclear primitives can be formed, it is hard to carbonize soy flour to form C-dots. However, powder on the microscale will be formed due to excessive carbonation if temperature is too high (Wu et al. 2015). In this work, as the reaction temperature increases from 160 to 200 °C, the fluorescent quantum yield of C-dots was sharply enhanced from 4.29 to 7.85 % (Table S1). However, the QY of CDs-240 (8.98 %) is only slightly increased (Table S1). Considering the energy consumption, 200 °C was selected as the optimized reaction temperature.

Structural characterization of CDs-200

The morphology and structure of C-dots were investigated by TEM, XRD, Raman spectroscopy, and NMR measurements. TEM image of CDs-200 (Fig. 2a) shows that the C-dots are well dispersed with an average diameter of 2.5 nm and the particle size distribution of the CDs-200 (Fig. 2b) is 1.5–4.0 nm. The high-resolution TEM (HRTEM) image of CDs-200 (Fig. 2a inset) shows well-resolved lattice fringes with an interplanar spacing of 0.21 nm, which is close to the (100) diffraction facet of graphite carbon (Guo et al. 2012). It suggests that the C-dots prepared via hydrothermal treatment method using soy flour have highly crystalline nature. The XRD spectrum of CDs-200 demonstrates that a broader and low-intensity diffraction peak centers at $2\theta = 20.12°$ with a calculated interlayer spacing of 0.44 nm (Fig. 3a), revealing a graphite carbon phase. The

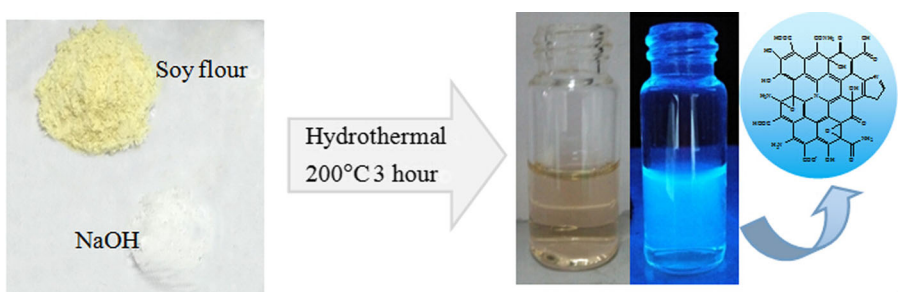

Fig. 1 Schematic illustration of the preparation procedure of C-dots by hydrothermal treatment from soy flour

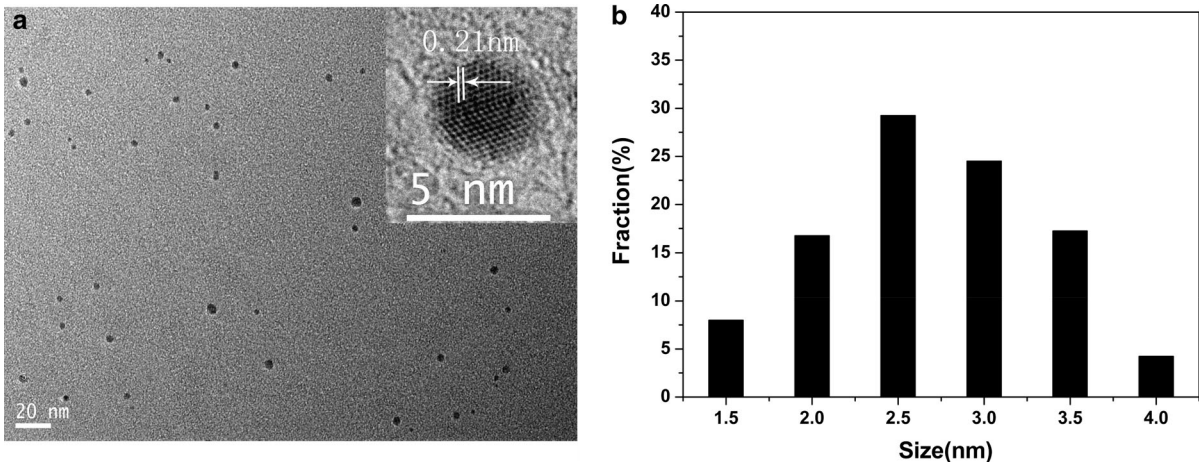

Fig. 2 **a** TEM image, *inset* HRTEM image, and **b** particle size distribution of CDs-200

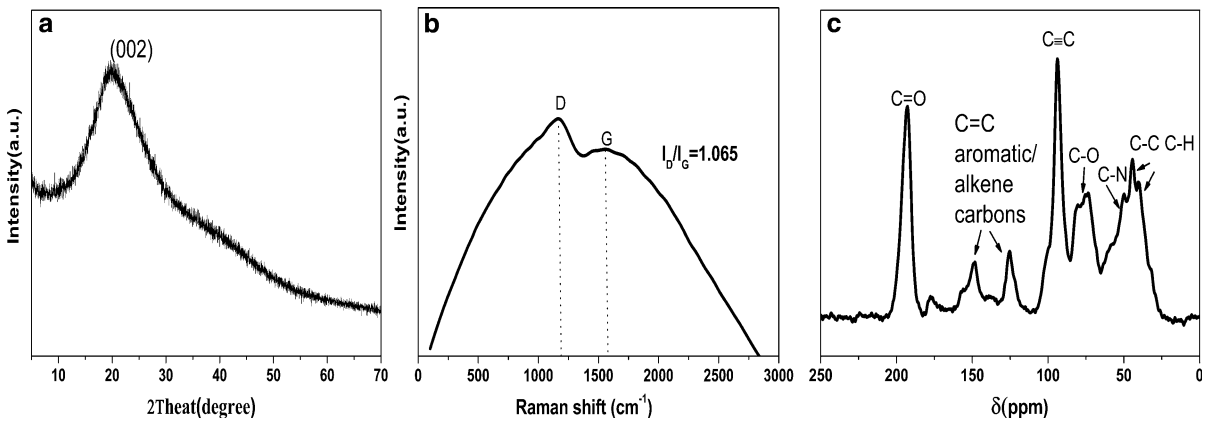

Fig. 3 **a** XRD spectrum, **b** Raman spectrum, and **c** ^{13}C NMR spectrum of CDs-200

interlayer spacing (0.44 nm) is larger than that of bulk graphite (0.34 nm) (Li et al. 2012), which may be attributed to the introduction of oxygen-containing groups and nitrogen-containing groups in the as-synthesized C-dots. The introductions of functionalized groups increase the structural defects of C-dots, which is beneficial for the fluorescent emission (vide infra). At the same time, the Raman spectrum of CDs-200 displays broader prominent Raman feature D and G bands. The D-band that centers at 1191 cm^{-1} arises from the extent of defects of sp^3 carbon atoms, and the G-band at 1565 cm^{-1} is attributed to the sp^2 carbon atoms (Zhou et al. 2007) (Fig. 3b). The intensity ratio of the characteristic D and G bands (I_D/I_G), a measurement of the disorder extent, can be associated with the structural properties of carbon. The I_D/I_G (1.065) of the as-prepared C-dots with graphite-like structure is much larger than that of graphite structure (0.365) (Li et al. 2012), suggesting that the higher I_D/I_G ratio may be caused by the increased disorder due to the introduction of C–N bands and amino groups on the surface of C-dots (Liu and Wu 2013), which is consistent with XRD results. ^{13}C NMR spectrometry is a powerful analysis technique in distinguishing sp^2 carbons and the sp^3 ones, which was measured to further gain the structural details about C-dots. The ^{13}C NMR spectrum of CDs-200 (Fig. 3c) shows C–C and C–H carbons in the range of 8–50 ppm, C–N carbons from 40 to 65 ppm, C–O carbons from 50 to 80 ppm, C=C aromatic/alkene carbons from 100 to 150 ppm, and C=O carbonyl/carboxylic carbons from 170 to 190 ppm. The results

reveal that the as-prepared C-dots contain a large amount of sp^3 carbon, such as C–C, C–N, and C–O.

The surface structure and components of C-dots were characterized by FT-IR, XPS, and elemental analyses. In the FT-IR spectrum of CDs-200 (Fig. 4a), there is a broad characteristic absorption band of O–H stretching vibration at around 3438 cm^{-1} (Jiang et al. 2012). The small bands at 2974 and 2922 cm^{-1} are due to the C–H stretching vibration (Feng et al. 2014). The peak at 1634 cm^{-1} is attributed to the C=O stretching vibration. The peak at 1532 cm^{-1} can be attributed to the Amide II band N–H bond. The peak at 1440–1400 cm^{-1} is considered to be the characteristic stretch band of the amine III C–N bond (Yang et al. 2014). In addition, the peak at 1250 cm^{-1} can be attributed to the C–N stretching vibration of amine. The peak at 1045 cm^{-1} is assigned to C–O–C and C–O bonds (Peng and Travas-Sejdic 2009). Obviously, the functional groups can be ascribed to the degradation of sugar, proteins, and lipids of soy flour via hydrothermal treatment. The structural defects and the elemental composition of the as-synthesized C-dots were further investigated by XPS characterization. XPS survey spectrum of CDs-200 (Fig. 4b) shows that they contain three dominant peaks: C_{1s} (around 285.1 eV), N_{1s} (around 400.9 eV), and O_{1s} (around 532 eV). In detail, the high-resolution C_{1s} XPS spectrum of CDs-200 (Fig. 4c) reveals four peaks with the binding energies of 284.6, 285.1, 286.2, and 288.0 eV ascribed to C–C=C, C–N, C–O, and C=O species, respectively (Bourlinos et al. 2008). The O_{1s} spectrum of CDs-200 has two peaks at 531.6 and 532.5 eV, which are attributed to the C=O and C–O in Fig. 4d, respectively. The N_{1s} spectrum of CDs-200 (Fig. 4e) has three peaks at 399.9, 400.6, and 401.6 eV, which could be ascribed to the pyridine N, pyrrolic N, and N–H, respectively (Wang et al. 2010a). The corresponding analytical results are displayed in Table S3, 4, 5.

Thus, the above results imply that the as-prepared C-dots most likely consist of nanocrystalline core with sp^2 and sp^3 carbons and functionalized surface with

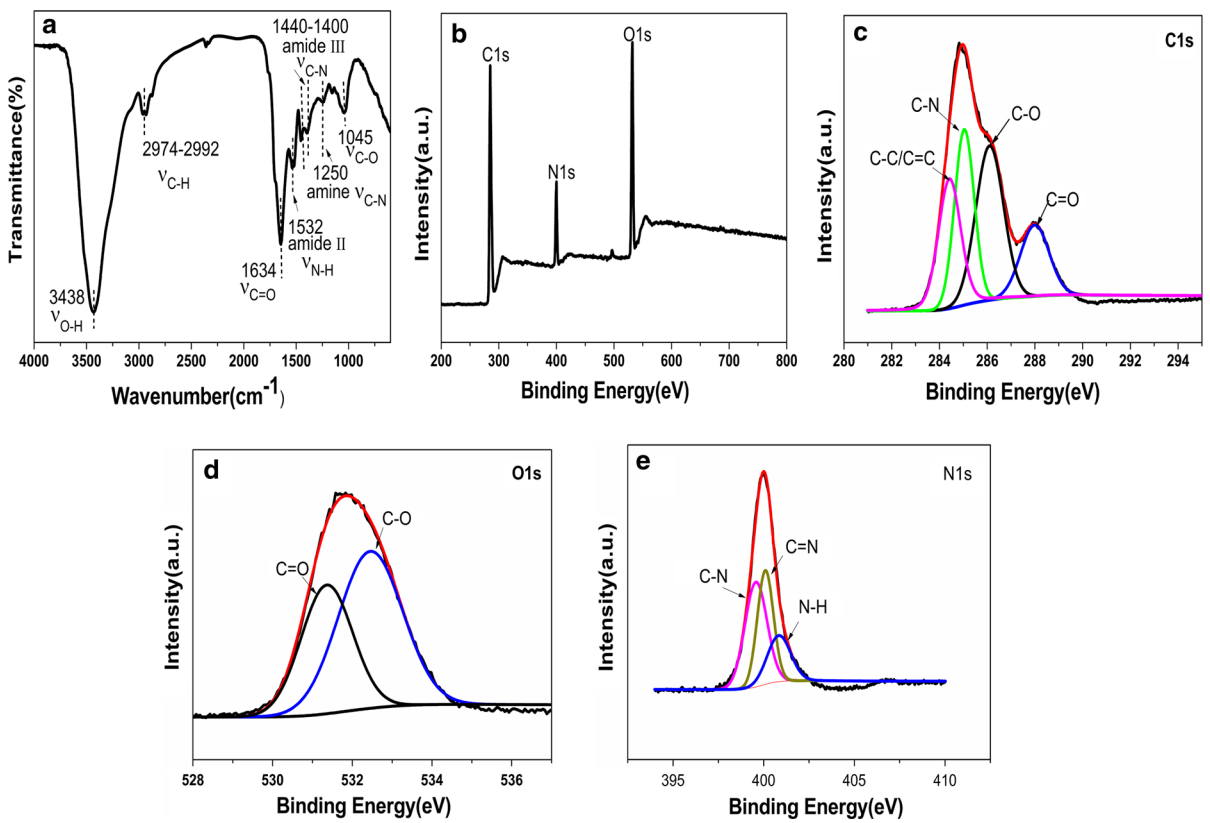

Fig. 4 **a** FT-IR spectrum, **b** XPS survey spectrum, **c** C_{1s} spectrum, **d** O_{1s} spectrum, and **e** N_{1s} spectrum of CDs-200

plentiful hydroxyl, carboxyl, amino, and amide groups. Consequently, the introductions of a large number of functional groups into the as-prepared C-dots increase the structural defects of C-dots, which can enhance the fluorescent emission.

Optical properties of CDs-200

The photographs of aqueous solution of CDs-200 with good water solubility are shown in Fig. 1. It shows yellow transparent liquid appearance in daylight, while it exhibits blue color fluorescence under the irradiation of 365 nm ultraviolet (UV) light lamp. Firstly, the ultraviolet–visible (UV–Vis) absorption spectrum of CDs-200 (Fig. 5a) exhibits characteristic absorption near 200 nm, a very broad absorption band in UV–Vis region due to the $\pi \rightarrow \pi^*$ transition of aromatic sp^2 domains with a tail extending to the visible light region (Sun et al. 2006; Zhu et al. 2009). Furthermore, a shoulder absorption peak at about 270 nm can also be observed, which is ascribed to the $n \rightarrow \pi^*$ transition of C=O (Nie et al. 2014). In the photoluminescence (PL) emission spectra (Fig. 5b), the maximum emission wavelength shifts from 399 to 510 nm as the excitation wavelengths increase from 290 to 470 nm. Simultaneously, the intensity first increases and then decreases. The emission of CDs-200 depends on the excitation wavelength, suggesting a superposition of various types of fluorescent species, which is a universal phenomenon observed in fluorescent carbon-based nanomaterials (Bao et al. 2011; Fang et al. 2012; Jeong et al. 2009; Liu et al. 2009; Loh et al. 2010; Wang et al. 2010b). In Fig. 5c, CDs-200 present the maximum emission peak at 440 nm

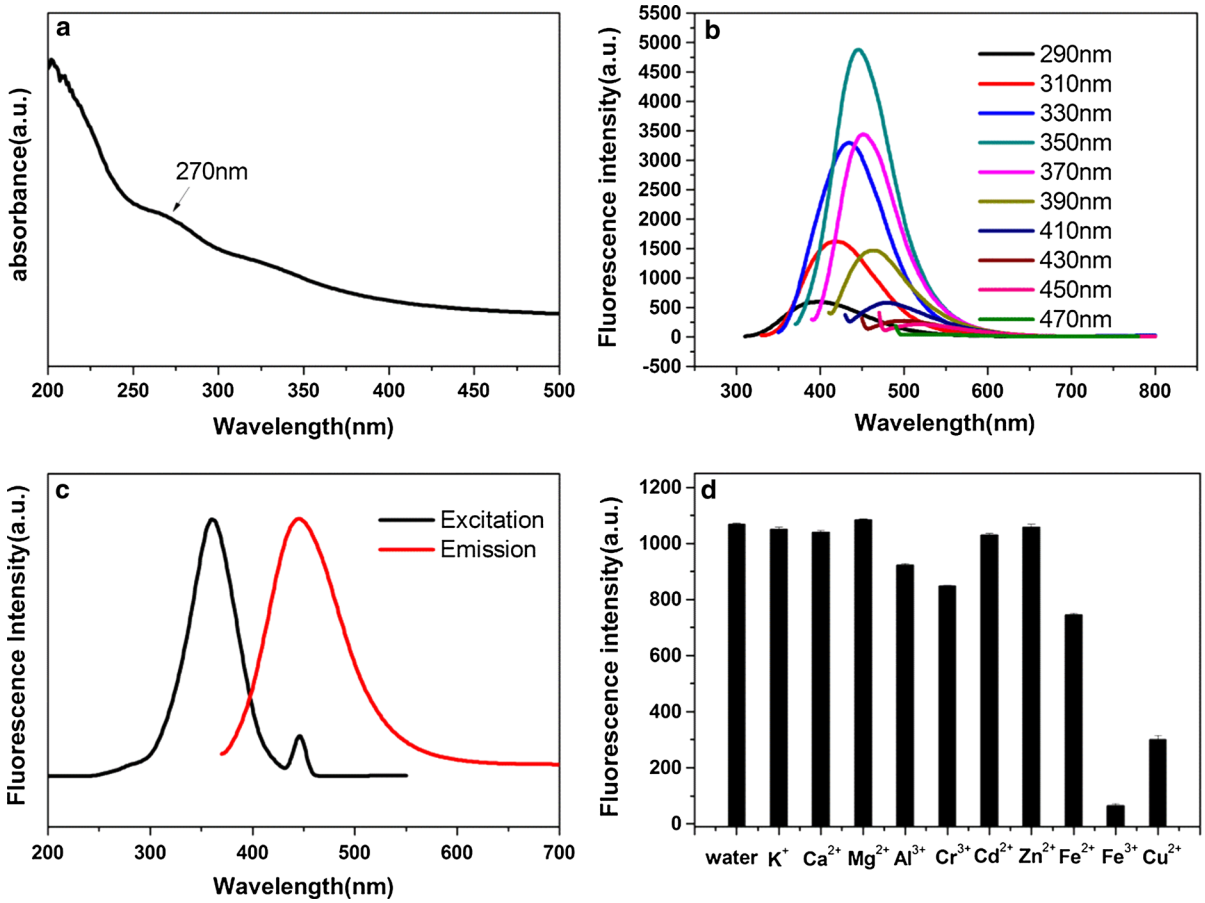

Fig. 5 **a** UV–Vis absorption spectrum, **b** PL spectra at different excitation wavelengths, and **c** optimal excitation and emission of PL spectra of CDs-200. **d** PL intensity of CDs-200 in the presence of the aqueous solution of various metal ions ($\lambda ex = 350$ nm; $[M^{n+}] = 10$ μM)

(λex = 350 nm), which is in accordance with the report that nitrogen-doped C-dots possess the strongest emission peak in the visible range (>400 nm) (Liu et al. 2012; Wu et al. 2013; Yang et al. 2011).

In addition to the excitation-dependent photoluminescence behavior of the C-dots, the fluorescent properties under various conditions were further studied. Fluorescent intensity of CDs-200 is not significantly decreased under continuous UV irradiation for 5 h (Figure S3) or in ambient air at room temperature for 4 months (Figure S4), which shows that CDs-200 are highly resistant to photobleaching property and outstanding optical stability. Fluorescence properties have no obvious changes in various concentrations of NaCl aqueous solution (Figure S5), which indicates that the emission behavior of CDs-200 is not dependent on the ionic strength of the medium. In the meantime, the PL emission intensity of the C-dots has almost no change in the pH range from 4 to 9 and slightly decreases at pH from 9 to 14 (Figure S6), suggesting that CDs-200 have good stability in a larger pH range. It is also observed that the intensity sharply decreases in the pH range from 4 to 1 due to amide hydrolysis at low pH, which implies that the decreased amide is not conducive to fluorescence emission. Furthermore, it is observed that CDs-200 are easily soluble in other polar solvents such as methanol and N,N-dimethylformamide (DMF) besides in water but poorly dissolved in nonpolar solvents such as cyclohexane and methylene chloride. The hydrogen bonds formed between nonbonding n electrons of hydrophilic groups of the C-dots and polar solvents can strengthen fluorescence emission. Thus, the fluorescence intensity of the C-dots in polar solution is stronger than that in nonpolar solution (Figure S7). Particularly, it is also found that the PL emission of the C-dots can be quenched effectively by some metal ions in solution. The effects of metal ions including K^+, Zn^{2+}, Ca^{2+}, Mg^{2+}, Fe^{2+}, Cu^{2+}, Cd^{2+}, Al^{3+}, Fe^{3+}, and Cr^{3+} on the fluorescence intensity of C-dots were investigated. Figure 5d shows that the fluorescence of CDs-200 is not very sensitive to most metal cations (at a concentration of 1.0×10^{-5} M). However, only Fe^{3+} and Cu^{2+} can effectively quench the fluorescence of CDs-200, especially Fe^{3+} shows stronger fluorescence quenching ability than Cu^{2+}, suggesting good selectivity of the C-dots for Fe^{3+}.

Therefore, combining the high photostability with good selectivity for Fe^{3+}, the as-prepared C-dots with attractive PL properties have promising application prospect in serving as a good fluorescence probe candidate in ferric ion detection.

Tuning structural defects to enhance fluorescence

In order to study the relationship of structural defects and fluorescence enhancement of C-dots, the influence of the synthesis temperature was investigated first. C-dots obtained at different preparation temperatures show similar particle size (Table S1; Figure S8, 9), indicating that the different emission properties are derived from other factors, such as the structural defects. Element analysis shows that the carbon and nitrogen contents of the as-prepared C-dots increase gradually (Table S2), suggesting that more O and N atoms are intercalated into the carbon backbone in the process of carbonization as the synthesis temperature increases. Figure 6a shows that the infrared characteristic absorption peaks of C–N and N–H around 1390–1590 cm^{-1} are obviously enhanced with the increase of temperature, implying that more nitrogen groups are formed in the C-dots when the synthesis temperature rises. Further, XPS C1 s (Fig. 6b Table S4) displays that the relative percentage contents of C–N in four different carbons of CDs-160 (25.81 %), CDs-200 (29.34 %), and CDs-240 (38.30 %) gradually increase. On the contrary, the relative percentage contents of C–O in four different carbons of the CDs-160 (37.34 %), CDs-200 (32.20 %), and CDs-240 (20.50 %) gradually decrease, and the relative percentage contents of C=O in four different carbons of the three kinds of C-dots also gradually decrease from 10.54 to 8.89 to 8.76 %. N1 s comparison chart (Fig. 6c Table S5) shows that the relative percentage contents of N–H in three different nitrogens of CDs-160 (7.50 %), CDs-200 (12.54 %), and CDs-240 (14.24 %) gradually increase. The influences of synthesis temperature on fluorescence emission properties of the as-prepared C-dots are revealed in Figure S10 and Table S1. It is found that their fluorescence intensity increases gradually and their quantum yields enlarge accordingly as the synthesis temperature increases. Obviously, N defects and O defects are successfully tuned by varying the synthesis temperature, leading to fluorescence intensity change of C-dots. Therefore, it is presumed that the increase of C–N and N–H structural

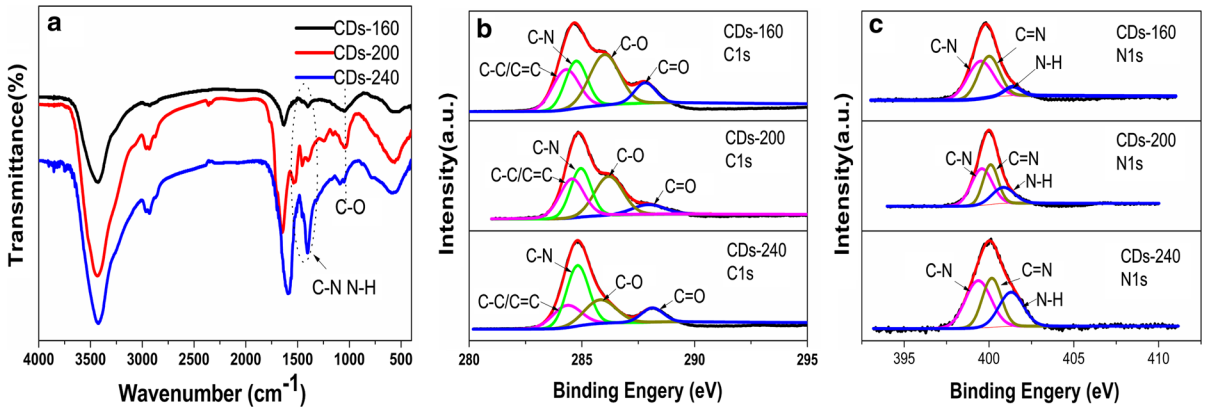

Fig. 6 **a** FT-IR spectra, **b** XPS C1 s spectra, and **c** XPS N1 s spectra of CDs-160, CDs-200, and CDs-240

defects may more efficiently enhance fluorescence emission than C–O and C=O structural defects.

In order to confirm the influence of N defects on the emission properties, CDs-200 were modified with ethylenediamine (reflux boiling with ethylenediamine at 120 °C for 8 h, denoted p-CDs). The QY of p-CDs is improved to 18.00 %, which is 2.3 times higher than that of CDs-200 (Table S1). Elemental analysis shows that the nitrogen content of p-CDs is 19.76 %, far higher than that of CDs-200 (9.98 %) (Table S2). In FT-IR comparison figure (Fig. 7a), the intensity of C–N bond of p-CDs obviously strengthens and the intensity of C–O, C=O, and O–H decreases, suggesting that the previously existed C–O–C and –COOH groups are replaced by –CONHR and –CNHR. C–O–C group and carboxyl group are thought to induce nonradiative recombination of localized electron–hole pairs (Mei et al. 2010). XPS spectra and the relative percentage contents of the different structural defects of CDs-200 and p-CDs are displayed in Fig. 7b, c, d and Table S3, 4, 5, respectively. As shown in XPS data, after surface passivation, the N/C atomic ratio has increased significantly from 0.1829 to 0.3385, and the change in O/C atomic ratio from 0.3127 to 0.3212 is inconspicuous (Fig. 7b; Table S3). The relative percentage contents of C–N in four different carbons of p-CDs (43.22 %) are higher than that of CDs-200 (29.34 %) (Fig. 7c; Table S4) and the relative percentage contents of N–H in three different nitrogens of p-CDs (16.47 %) are higher than that of CDs-200 (12.54 %) (Fig. 7d; Table S5). Consistent with the analysis of FT-IR spectra, these results obtained from XPS data also confirm that more C–N and N–H defects are formed by substituting for partial C–O and C=O defects in C-dots after surface passivation by ethylenediamine, resulting in the reduction of nonradiative recombination and fluorescence enhancement. It is noteworthy that, in UV–vis absorption spectra of the two kinds of C-dots (Fig. 7e), CDs-200 show an evident absorption peak at 270 nm (4.98 eV, $n \rightarrow \pi^*$ of C=O). However, the absorption peak in p-CDs exhibits obvious red-shift from 270 to 330 nm (3.76 eV), which may be due to the impact of the introduction of auxochrome (e.g., N–H) on chromophore (C=O) after surface passivation. To explain this phenomenon, the nonbonding n electrons of nitrogen are easily excited into the carbon ring to form p–π conjugate than that of oxygen because both n electron cloud of nitrogen-containing groups and π electron cloud of carbon ring are almost coplanar, which enlarge the electronic activity scope and lead to electron energy level transition to low energy (the red-shift of absorption peaks). As a result, the new $n \rightarrow \pi^*$ transition energy level (e.g., 3.76 eV) is introduced into the electronic structures of C-dots. Subsequently, the excited electrons from π^* orbital can relax to the $n_{(N)}$ ground states by radiative relaxation (Wu 2014), forming more radiative recombination and enhancing fluorescence emission. Figure 8 schematically illustrates the fluorescence enhancement mechanism of the as-prepared C-dots.

From the discussion above, the C–N and N–H defects were finely tuned by substituting for partial O defects, enhancing the fluorescence intensity, and reducing nonradiative recombination. It is further proven that C–N and N–H defects have greater influence on fluorescent intensity than C–O and O–H defects.

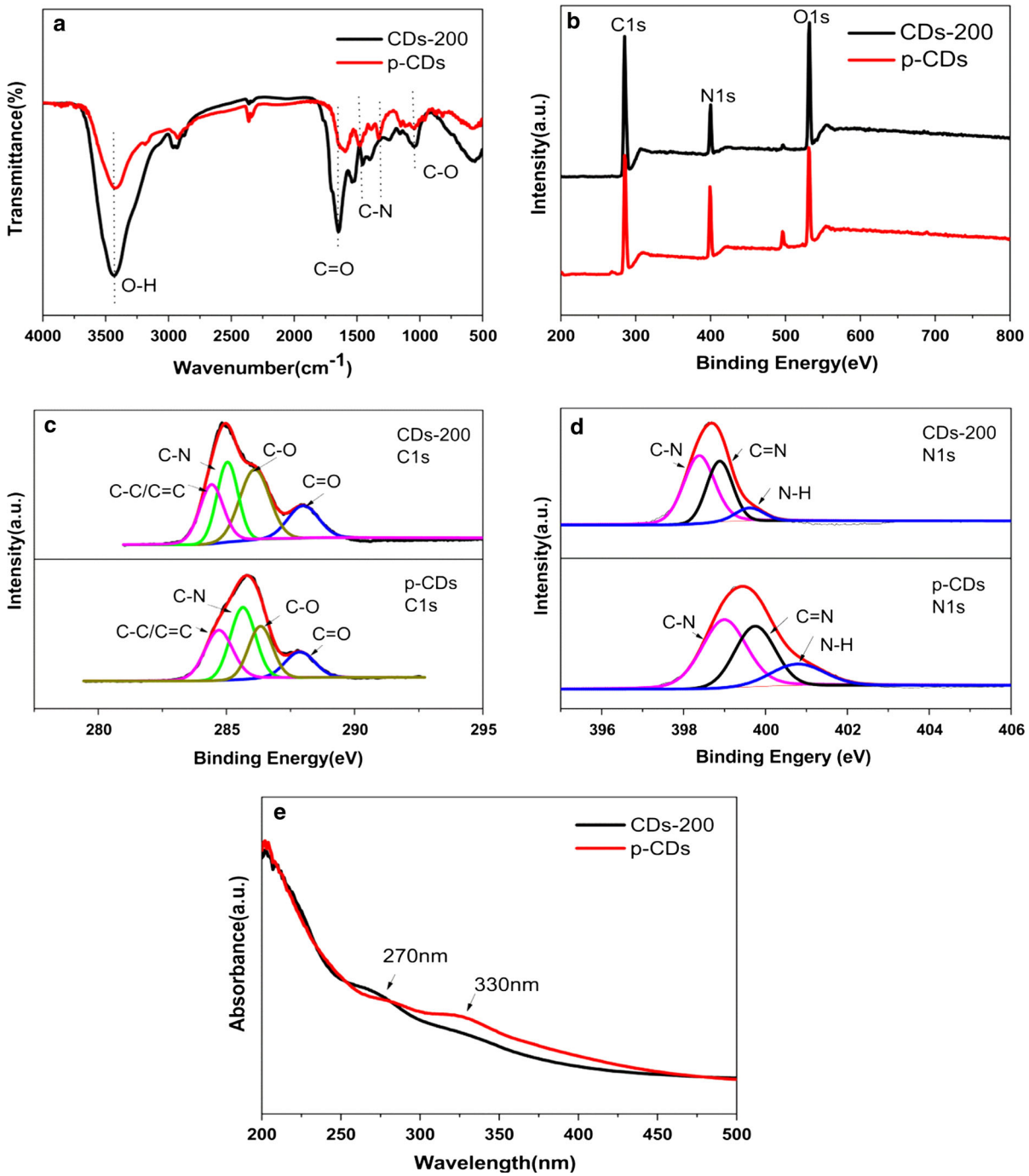

Fig. 7 **a** FT-IR spectra, **b** XPS survey spectra, **c** C_{1s} spectra, **d** N_{1s} spectra, **e** ^{13}C NMR spectra, and **f** UV–Vis absorption spectra of CDs-200 and p-CDs

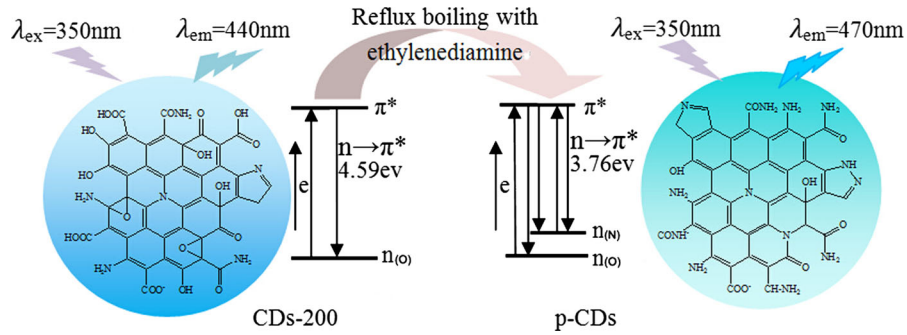

Fig. 8 Schematic illustration of fluorescence enhancement mechanism of the as-prepared C-dots

Effect of ferric ion on the fluorescence intensity of C-dots

CDs-200 can be used for ferric ion detection since Fe^{3+} can effectively quench the fluorescence of CDs-200. From the previous discussion in Sect. "Optical properties of CDs-200" (Fig. 5d), we can learn that the fluorescence of CDs-200 cannot be effectively quenched by most metal cations such K^+, Zn^{2+}, Ca^{2+}, Mg^{2+}, Fe^{2+}, Cr^{3+}, Cd^{2+}, and Al^{3+} except Fe^{3+} and Cu^{2+}. Particularly, the outstanding fluorescence quenching ability of ferric ions suggests that CDs-200 have good selectivity for Fe^{3+}.

Fluorescence quenching of CDs-200 by ferric ion may be attributed to its ion-selective chemical structure (Sun et al. 2010) that could facilitate the electron/hole recombination annihilation through an effective electron transfer process. CDs-200 contain a large number of hydroxyl, carboxyl, amino, and amide groups and offer the possibility of forming complex heterocyclic compounds such as certain fluorescent recognition groups (e.g., quinoline (Li et al. 2009; Seung Lee et al. 2002) and acridine (Lee et al. 2000)) that play a very important role in the selectivity of ferric ion (Sun et al. 2010), which facilitates the fluorescence quenching of CDs-200 by ferric ions. Compared with other transition metals, Cu^{2+} has stronger binding force and chelating power to –COO– (Sun et al. 2013b). CDs-200 contain more nitrogen functional groups than the oxygen functional groups (from the previous discussion). Therefore, we speculate that it may be easier for CDs-200 to bind Fe^{3+} than Cu^{2+}, showing stronger fluorescence quenching ability by Fe^{3+}.

Figure 9a shows the fluorescence intensity of CDs-200 in the presence of different concentrations of Fe^{3+} in Tris–HCl buffer (pH 7.0) solution with an excitation at 350 nm. CDs-200 show strong fluorescence in the absence of Fe^{3+} aqueous solution. With the increase of Fe^{3+} concentration, the fluorescence intensity of CDs-

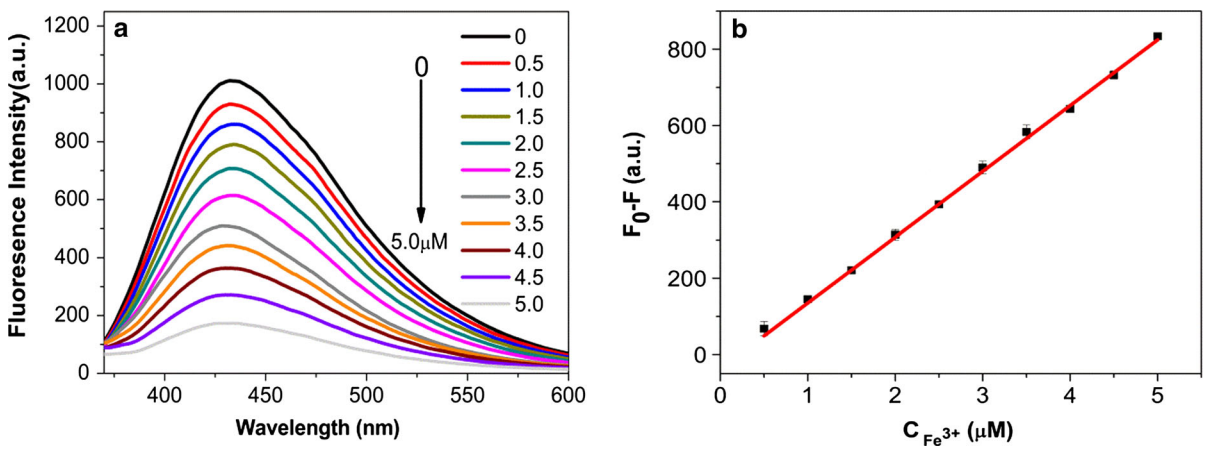

Fig. 9 **a** PL response of CDs-200 in the presence of different concentrations of Fe^{3+} in Tris–HCl buffer (pH 7.0) solution with an excitation at 350 nm. **b** *Plot* of the changes of fluorescence intensity F_0–F versus Fe^{3+} concentrations ranging from 0 to 5 μM

200 gradually reduces. When the concentration of Fe^{3+} reached 5.0 μM, CDs-200 fluorescence quenching rate achieved was 92 %. The experiment reveals that the PL intensity of CDs-200 is quenched by ferric ions in the range of 0–5.0 μM in a concentration-dependent manner, which can be well described by the linear regression equations: F_0–F = 172.31[C]–37.02 with a correlation coefficient of 0.9994 (Fig. 9b). Here F_0 and F represent the PL intensity of CDs-200 in the absence and presence of Fe^{3+}, respectively, and [C] is the Fe^{3+} concentration. The detection limit of 0.021 μM is obtained based on 3σ/k (σ is the standard deviation of the blank signal and k is the slope of the linear calibration plot), which is lower than the values reported in most of the previous experiments for Fe^{3+} detection (Arundithi et al. 2014; Dong et al. 2010), suggesting that the CDs-200 possess good sensitivity for the detection of trace ferric.

From what has been discussed above, the as-prepared C-dots can be successfully used as fluorescence probes for detecting the concentrations of ferric ion.

Conclusion

In summary, we successfully synthesized high-quality soy flour-derived C-dots via a facile one-step hydrothermal approach. As the preparation temperature increases, the C–N and N–H defects are fine-tuned to reduce nonradiative recombination and enhance fluorescence intensity, which are further confirmed by surface passivation. The as-prepared C-dots exhibit an average diameter of 2.5 nm and the crystalline lattices are consistent with graphitic carbons. Meanwhile, they show good water solubility, strong photoluminescence, and high photostability. Due to its high sensitivity and good selectivity for Fe^{3+}, the as-prepared C-dots were used as fluorescence probes for detection of ferric ion, the detection limitation comes to 0.021 μM.

Acknowledgments This work is financially supported by the National Natural Science Foundation of China (Grant No. 21376268) and the Fundamental Research Funds for the Central Universities (No. 15CX08005A).

References

Arundithi A, Wang X, Parimal R, Barindra S, Sierin L, Dong Hwan K, Kok Hwa L, Li J, Chen P (2014) Facile synthesis of graphene quantum dots from 3D graphene and their application for Fe^{3+} Sensing. Adv Funct Mater 24(20): 3021–3026. doi:10.1002/adfm.201303441

Bai W, Zheng H, Long Y, Mao X, Gao M, Zhang L (2011) A carbon dots-based fluorescence turn-on method for DNA Determination. Anal Sci 27(3):243. doi:10.2116/analsci.27.243

Baker SN, Baker GA (2010) Lumineszierende Kohlenstoff-Nanopunkte: Nanolichtquellen mit Zukunft. Angewandte Chemie 122(38):6876–6896. doi:10.1002/ange.200906623

Bao L, Zhang Z-L, Tian Z-Q, Zhang L, Liu C, Lin Y, Qi B, Pang D-W (2011) Electrochemical tuning of luminescent carbon nanodots: from preparation to luminescence mechanism. Adv Mater 23(48):5801–5806. doi:10.1002/adma.201102866

Bourlinos AB, Stassinopoulos A, Anglos D, Zboril R, Karakassides M, Giannelis EP (2008) Surface functionalized carbogenic quantum dots. Small 4(4):455–458. doi:10.1002/smll.200700578

Cao L, Sahu S, Anilkumar P, Bunker CE, Xu J, Fernando KAS, Wang P, Guliants EA, Tackett KN, Sun Y-P (2011) Carbon nanoparticles as visible-light photocatalysts for efficient CO2 conversion and beyond. J Am Chem Soc 133(13): 4754–4757. doi:10.1021/ja200804h

De B, Karak N (2013) A green and facile approach for the synthesis of water soluble fluorescent carbon dots from banana juice. Rsc Adv 3(22):8286–8290. doi:10.1039/C3RA00088E

Dong L, ChongWu X Zeng, Mu L, Xue SF, Tao Z, Zhang JX (2010) The synthesis of a rhodamine B schiff-base chemosensor and recognition properties for Fe^{3+} in neutral ethanol aqueous solution. Sens Actuators B Chem 145(1): 433–437. doi:10.1016/j.snb.2009.12.057

Dong Y, Li G, Zhou N, Wang R, Chi Y, Chen G (2012) Graphene quantum dot as a green and facile sensor for free chlorine in drinking water. Anal Chem 84(19):8378–8382. doi:10.1021/ac301945z

Fan Z, Li Y, Li X, Fan L, Zhou S, Fang D, Yang S (2014) Surrounding media sensitive photoluminescence of boron-doped graphene quantum dots for highly fluorescent dyed crystals, chemical sensing and bioimaging. Carbon 70: 149–156. doi:10.1016/j.carbon.2013.12.085

Fang Y, Guo S, Li D, Zhu C, Ren W, Dong S, Wang E (2012) Easy synthesis and imaging applications of cross-linked green fluorescent hollow carbon nanoparticles. ACS Nano 6(1):400–409. doi:10.1021/nn2046373

Feng Y, Zhao J, Yan X, Tang F, Xue Q (2014) Enhancement in the fluorescence of graphene quantum dots by hydrazine hydrate reduction. Carbon 66:334–339. doi:10.1016/j.carbon.2013.09.008

Guo X, Wang C-F, Yu Z-Y, Chen L, Chen S (2012) Facile access to versatile fluorescent carbon dots toward light-emitting diodes. Chem Commun 48(21):2692–2694. doi:10.1039/C2CC17769B

Hu Y, Yang J, Tian J, Jia L, Yu J-S (2014) Waste frying oil as a precursor for one-step synthesis of sulfur-doped carbon dots with pH-sensitive photoluminescence. Carbon 77: 775–782. doi:10.1016/j.carbon.2014.05.081

Jeong J, Cho M, Lim YT, Song NW, Chung BH (2009) Synthesis and Characterization of a Photoluminescent Nanoparticle Based on Fullerene-Silica Hybridization.

Angewandte Chemie 48(29):5296–5299. doi:10.1002/anie.200901750

Jiang J, He Y, Li S, Cui H (2012) Amino acids as the source for producing carbon nanodots: microwave assisted one-step synthesis, intrinsic photoluminescence property and intense chemiluminescence enhancement. Chem Commun 48(77):9634–9636. doi:10.1039/C2CC34612E

Jung J, Solanki A, Memoli KA, K-i Kamei H, Kim MA Drahl, Williams LJ, Tseng H-R, Lee K (2010) Selective inhibition of human brain tumor cells through multifunctional quantum-dot-based siRNA delivery. Angewandte Chemie 122(1):107–111. doi:10.1002/ange.200905126

Lee TS, Yang C, Park WH (2000) Synthesis and electrostatic multilayer assembly of an acridine-containing polymer with properties of an optical sensor. Macromol Rapid Commun 21(14):951–955. doi:10.1002/1521-3927(20000901)21:14<951:AID-MARC951>3.0.CO;2-N

Li N, Xu Q, Xia X, Wang L, Lu J, Wen X (2009) A polymeric chemosensor for Fe^{3+} based on fluorescence quenching of polymer with quinoline derivative in the side chain. Mater Chem Phys 114(1):339–343. doi:10.1016/j.matchemphys.2008.09.027

Li H, He X, Kang Z, Huang H, Liu Y, Liu J, Lian S, Tsang CHA, Yang X, Lee S-T (2010) Water-soluble fluorescent carbon quantum dots and photocatalyst design. Angewandte Chemie 49(26):4430–4434. doi:10.1002/anie.200906154

Li H, Kang Z, Liu Y, Lee S-T (2012) Carbon nanodots: synthesis, properties and applications. J Mater Chem 22(46):24230–24253. doi:10.1039/C2JM34690G

Li X, Zhang S, Kulinich SA, Liu Y, Zeng H (2014) Engineering surface states of carbon dots to achieve controllable luminescence for solid-luminescent composites and sensitive Be^{2+} detection. Sci Rep 4(2):4976–4984. doi:10.1038/srep04976

Liu Y, Wu P (2013) Graphene quantum dot hybrids as efficient metal-free electrocatalyst for the oxygen reduction reaction. ACS Appl Mater Interfaces 5(8):3362–3369. doi:10.1021/am400415t

Liu R, Wu D, Liu S, Koynov K, Knoll W, Li Q (2009) An aqueous route to multicolor photoluminescent carbon dots using silica spheres as carriers. Angewandte Chemie 121(25):4668–4671. doi:10.1002/ange.200900652

Liu S, Tian J, Wang L, Zhang Y, Qin X, Luo Y, Asiri AM, Al-Youbi AO, Sun X (2012) Hydrothermal treatment of grass: a low-cost, green route to nitrogen-doped, carbon-rich, photoluminescent polymer nanodots as an effective fluorescent sensing platform for label-free detection of Cu(II) ions. Adv Mater 24(15):2037–2041. doi:10.1002/adma.201200164

Loh KP, Bao Q, Eda G, Chhowalla M (2010) Graphene oxide as a chemically tunable platform for optical applications. Nat Chem 2(12):1015–1024. doi:10.1038/nchem.907

Lu W, Qin X, Liu S, Chang G, Zhang Y, Luo Y, Asiri AM, Al-Youbi AO, Sun X (2012) Economical, green synthesis of fluorescent carbon nanoparticles and their use as probes for sensitive and selective detection of mercury(II) ions. Anal Chem 84(12):5351–5357. doi:10.1021/ac3007939

Mei Q, Zhang K, Guan G, Liu B, Wang S, Zhang Z (2010) Highly efficient photoluminescent graphene oxide with tunable surface properties. Chem Commun 46(39):7319–7321. doi:10.1039/c0cc02374d

Nie H, Li M, Li Q, Liang S, Tan Y, Sheng L, Shi W, Zhang SX-A (2014) Carbon dots with continuously tunable full-color emission and their application in ratiometric ph sensing. Chem Mater 26(10):3104–3112. doi:10.1021/cm5003669

Peng H, Travas-Sejdic J (2009) Simple aqueous solution route to luminescent carbogenic dots from carbohydrates. Chem Mater 21(23):5563–5565. doi:10.1021/cm901593y

Qu Q, Zhu A, Shao X, Shi G, Tian Y (2012) Development of a carbon quantum dots-based fluorescent Cu^{2+} probe suitable for living cell imaging. Chem Commun 48(44):5473–5475. doi:10.1039/C2CC31000G

Sahu S, Behera B, Maiti TK, Mohapatra S (2012) Simple one-step synthesis of highly luminescent carbon dots from orange juice: application as excellent bio-imaging agents. Chem Commun 48(70):8835–8837. doi:10.1039/C2CC33796G

Seung Lee T, Yang C, Kim JL, Lee J-K, Park WH, Won Y (2002) Synthesis of polyquinoline ether and its optical sensor property in the presence of metal cations. J Polym Sci Part A Polym Chem 40(11):1831–1837. doi:10.1002/pola.10270

Sun Y-P, Zhou B, Lin Y, Wang W, Fernando KAS, Pathak P, Meziani MJ, Harruff BA, Wang X, Wang H, Luo PG, Yang H, Kose ME, Chen B, Veca LM, Xie S-Y (2006) Quantum-sized carbon dots for bright and colorful photoluminescence. J Am Chem Soc 128(24):7756–7757. doi:10.1021/ja062677d

Sun W, Du Y, Wang Y (2010) Study on fluorescence properties of carbogenic nanoparticles and their application for the determination of ferrous succinate. J Lumin 130(8):1463–1469. doi:10.1016/j.jlumin.2010.03.013

Sun D, Ban R, Zhang PH, Wu GH, Zhang JR, Zhu JJ (2013a) Hair fiber as a precursor for synthesizing of sulfur- and nitrogen-co-doped carbon dots with tunable luminescence properties. Carbon 64:424–434. doi:10.1016/j.carbon.2013.07.095

Sun H, Gao N, Wu L, Ren J, Wei W, Qu X (2013b) Highly photoluminescent amino-functionalized graphene quantum dots used for sensing copper ions. Chemistry 19(40):13362–13368. doi:10.1002/chem.201302268

Wang F, Pang S, Wang L, Li Q, Kreiter M, Liu C-y (2010a) One-step synthesis of highly luminescent carbon dots in noncoordinating solvents. Chem Mater 22(16):4528–4530. doi:10.1021/cm101350u

Wang X, Cao L, Yang S-T, Lu F, Meziani MJ, Tian L, Sun KW, Bloodgood MA, Sun Y-P (2010b) Bandgap-like strong fluorescence in functionalized carbon nanoparticles. Angewandte Chemie 122(31):5438–5442. doi:10.1002/ange.201000982

Wu ZL, Zhang P, Gao MX, Liu CF, Wang W, Leng F, Huang CZ (2013) One-pot hydrothermal synthesis of highly luminescent nitrogen-doped amphoteric carbon dots for bioimaging from Bombyx mori silk–natural proteins. J Mater Chem B 1(22):2868–2873. doi:10.1039/C3TB20418A

Wu M, Wang Y, Wu W, Hu C, Wang X, Zheng J, Li Z, Jiang B, Qiu J (2014) Preparation of functionalized water-soluble photoluminescent carbon quantum dots from petroleum coke. Carbon 78:480–489. doi:10.1016/j.carbon.2014.07.029

Wu W, Zhan L, Fan W, Song J, Li X, Li Z, Wang R, Zhang J, Zheng J, Wu M (2015) Cu–N dopants boost electron

transfer and photooxidation reactions of carbon dots. Angewandte Chemie 127(22):6640–6644. doi:10.1002/anie.201501912

Xu Q, Liu Y, Gao C, Wei J, Zhou H, Chen Y, Dong C, Sreeprasad TS, Li N, Xia Z (2015) Synthesis, mechanistic investigation, and application of photoluminescent sulfur and nitrogen co-doped carbon dots. J Mater Chem C 3(38):9885–9893. doi:10.1039/C5TC01912E

Yang Z-C, Li X, Wang J (2011) Intrinsically fluorescent nitrogen-containing carbon nanoparticles synthesized by a hydrothermal process. Carbon 49(15):5207–5212. doi:10.1016/j.carbon.2011.07.038

Yang Z, Xu MH, Liu Y, He FJ, Gao F, Su YJ, Wei H, Zhang YF (2014) Nitrogen-doped, carbon-rich, highly photoluminescent carbon dots from ammonium citrate. Nanoscale 6(3):1890–1895. doi:10.1039/c3nr05380f

Zhang M, Bai L, Shang W, Xie W, Ma H, Fu Y, Fang D, Sun H, Fan L, Han M, Liu C, Yang S (2012) Facile synthesis of water-soluble, highly fluorescent graphene quantum dots as a robust biological label for stem cells. J Mater Chem 22(15):7461–7467. doi:10.1039/C2JM16835A

Zheng L, Chi Y, Dong Y, Lin J, Wang B (2009) Electrochemiluminescence of water-soluble carbon nanocrystals released electrochemically from graphite. J Am Chem Soc 131(13):4564–4565. doi:10.1021/ja809073f

Zhou J, Booker C, Li R, Zhou X, Sham T-K, Sun X, Ding Z (2007) An electrochemical avenue to blue luminescent nanocrystals from multiwalled carbon nanotubes (MWCNTs). J Am Chem Soc 129(4):744–745. doi:10.1021/ja0669070

Zhou L, Lin Y, Huang Z, Ren J, Qu X (2012) Carbon nanodots as fluorescence probes for rapid, sensitive, and label-free detection of Hg^{2+} and biothiols in complex matrices. Chem Commun 48(8):1147–1149. doi:10.1039/C2CC16791C

Zhu H, Wang X, Li Y, Wang Z, Yang F, Yang X (2009) Microwave synthesis of fluorescent carbon nanoparticles with electrochemiluminescence properties. Chem Commun 34:5118–5120. doi:10.1039/B907612C

Zhu C, Zhai J, Dong S (2012a) Bifunctional fluorescent carbon nanodots: green synthesis via soy milk and application as metal-free electrocatalysts for oxygen reduction. Chem Commun 48(75):9367–9369. doi:10.1039/C2CC33844K

Zhu S, Zhang J, Tang S, Qiao C, Wang L, Wang H, Liu X, Li B, Li Y, Yu W, Wang X, Sun H, Yang B (2012b) Surface chemistry routes to modulate the photoluminescence of graphene quantum dots: from fluorescence mechanism to up-conversion bioimaging applications. Adv Funt Mater 22(22):4732–4740. doi:10.1002/adfm.201201499

Zhuo S, Shao M, Lee S-T (2012) Upconversion and downconversion fluorescent graphene quantum dots: ultrasonic preparation and photocatalysis. ACS Nano 6(2):1059–1064. doi:10.1021/nn2040395